Fast and tiny: A model for the flame propagation of nanopowders

Audrey Santandrea, David Torrado, Matteo Pietraccini, Alexis Vignes, Laurent Perrin, Olivier Dufaud

Fast and tiny : A model for the flame propagation of nanopowders

Audrey Santandrea [a,b], David Torrado [a], Matteo Pietraccini [a], Alexis Vignes [b], Laurent Perrin [a] & Olivier Dufaud [a]

[a] Université de Lorraine, CNRS, LRGP, F-54000 Nancy, France

[b] INERIS, Accidental Risks Division, Parc Technologique ALATA, Verneuil-en-Halatte, France

E-mail: olivier.dufaud@univ-lorraine.fr

Abstract

To avoid the influence of external parameters, such as the vessel volume or the initial turbulence, the explosion severity should be determined from intrinsic properties of the fuel-air mixture. Therefore, the flame propagation of gaseous mixtures is often studied in order to estimate their laminar burning velocity, which is both independent of external factors and a useful input for CFD simulation. Experimentally, this parameter is difficult to evaluate when it comes to dust explosion, due to the inherent turbulence during the dispersion of the cloud. However, the low inertia of nanoparticles allows performing tests at very low turbulence without sedimentation. Knowledge on flame propagation concerning nanoparticles may then be modelled and, under certain conditions, extrapolated to microparticles, for which an experimental measurement is a delicate task. This work focuses on a nanocellulose with primary fiber dimensions of 3 nm width and 70 nm length. A one-dimensional model was developed to estimate the flame velocity of a nanocellulose explosion, based on an existing model already validated for hybrid mixtures of gas and carbonaceous nanopowders similar to soot. Assuming the fast devolatilization of organic nanopowders, the chemical reactions considered are limited to the combustion of the pyrolysis gases. The finite volume method was used to solve the mass and energy balances equations and mass reactions rates constituting the numerical system. Finally, the radiative heat transfer was also considered, highlighting the influence of the total surface area of the particles on the thermal radiation. Flame velocities of nanocellulose from 17.5 to 20.8 cm/s were obtained numerically depending on the radiative heat transfer, which proves a good

agreement with the values around 21 cm/s measured experimentally by flame visualization and allows the validation of the model for nanoparticles.

Keywords: *dust explosion, flame propagation, nanoparticles, modeling*

1. Introduction

Safety barriers, such as explosion venting or suppression systems (Fauske and Clouthier, 2015) need to be designed by considering the experimental characteristics of the dust explosibility. These characteristics are routinely determined in a 20 L sphere (Zalosh, 2019) according to well established standards like EN 14034-1 (2004) and EN 14034-2 (2006). This approach only holds by assuming that dust explosibility can be represented by the maximum explosion overpressure value P_{max} and the K_{st} index, deduced from the maximum rate of pressure rise dP/dt_{max}. However, it needs to be further questioned as the measurement of dust explosion severity is actually influenced by several parameters such as the initial turbulence (Amyotte et al., 1988; Zhen and Leuckel, 1997), the ignition energy (Zhen and Leuckel, 1997), the moisture content of the powder (Traoré et al., 2009) and the type of dispersion nozzle (Dahoe et al., 2001; Murillo et al., 2018; Yao et al., 2020). Beyond these main influential factors, the validity of the so-called 'cubic law' (Dahoe et al., 2001) commonly used to extrapolate results obtained in a confined volume to another volume (Eckhoff, 2003) is also questioned.

Standard conditions were initially defined to evaluate the explosion severity of microparticles, but when it comes to nanoparticles, potential discrepancies can arise. Indeed, their small size induces a high specific area and new properties, which can lead to modifications in the combustion kinetics (Bouillard et al., 2010; Dufaud et al., 2011) along with extremely high ignition sensitivity, especially for metallic nanopowders that can spontaneously ignite when exposed to air (Boilard et al., 2013; Krietsch et al., 2015). An evaluation of the adequacy of the current standards for the assessment of the explosion severity of nanoparticles is then necessary (Santandrea et al., 2019b).

To overcome the identified limitations, direct investigation of the flame propagation could be useful so as to provide fundamental inputs in advanced simulations (CFD or phenomenological approach). An essential parameter is then the laminar burning velocity, which is an intrinsic property of the fuel-air mixture (Belerrajoul, 2019; Dahoe et al., 2002) that can be used in such simulations to evaluate the consequences of an explosion scenario in specific conditions (Skjold, 2003). The existence of a laminar burning velocity of dusts is difficult to define due to the inherent turbulence related to the dispersion of the powder but such an approach was already proposed 30 years ago by Bradley and Lee (1984), though it proved itself challenging when it comes to dusts. Nevertheless, the low inertia and sedimentation rate of nanoparticles enable to investigate flame propagation in very low turbulent conditions (Santandrea et al., 2020).

In this paper, a one-dimensional model initially conceived and validated for hybrid mixtures of gas and combustible dust (Torrado et al., 2018) has been modified and adapted to predict the laminar flame velocity of nanocellulose. Results of simulations are then compared to the experimental values measured on nanocellulose using a flame propagation tube and a vented explosion sphere (Santandrea et al., 2020). The consistency of a correlation established by Silvestrini et al. (2008) to predict laminar flame velocity of micropowders based on the knowledge of their explosion severity was also analyzed for nanocellulose.

2. Material and experimental method

2.1 Flame propagation observation

Nanocellulose powder, or more precisely a cellulose nanocrystals powder NCC (CelluForce), is composed of primary fibers, whose dimensions are 70 nm length and 3 nm width. The flame propagation of nanocellulose was studied at low turbulence by Santandrea et al. (2020) in a flame propagation tube (Cuervo et al., 2017) and in a vented visualization 20 L sphere, as summarized in Figure 1. Due to a difficult visualization of the flame kernel at high concentration, a concentration of 500 g/m^3 was chosen, as it is higher than the minimum explosible concentration, i.e. 125 g/m^3, to

ensure an ignition at low ignition energy. It is greater than 225 g/m^3, the theoretical stoichiometric concentration, and rather close to the experimental optimal concentration, i.e. 750 g/m^3. The particle size distribution of nanocellulose dispersed in both setups was determined in situ using a laser diffraction sensor (Helos - Sympatec). It appears that the mean surface diameter in the 20L sphere reaches 10 µm, 60 ms after the beginning of the dispersion. However, by applying lower dispersion stresses, e.g. by sedimentation, agglomerates ranging from a few micrometers up to 60 µm are formed in the powder. This does not exclude the presence of nanoparticles (from 100 nm to 300 nm) in the dust cloud as demonstrated by using a Fast Mobility Particle Sizer (FMPS) and a Scanning Mobility (Santandrea et al., 2020).

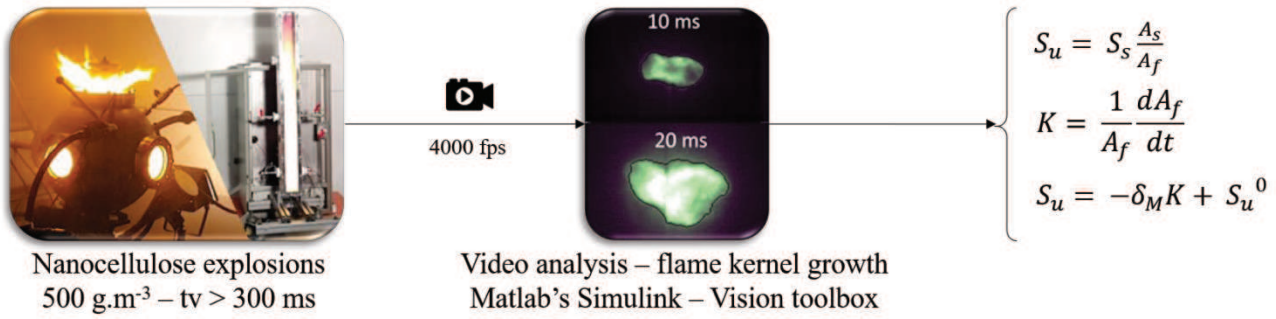

Figure 1. Simplified scheme of the experimental determination of the laminar burning velocity by flame visualization used by Santandrea et al. (2020)

Explosion were recorded using a high-speed video camera, and the flame kernel growth was analysed in terms of flame front position and surface area using a model developed by Cuervo (2015) in Matlab's Simulink. The equations initially established for gases were then applied to the obtained values, assuming that the devolatilization of organic nanopowders is fast and that, under certain concentration and turbulence conditions, the reaction is then limited by the combustion of the pyrolysis gases (Cuervo, 2015; Di Benedetto and Russo, 2007; Dufaud et al., 2012a). This regime corresponds to small particles for which both heating and pyrolysis steps occur very fast with regard to the gas combustion; i.e. for low pyrolysis time over gas combustion time ratio (Di Benedetto et al.,

2010). Thus, the burning velocity was calculated using the spatial velocity S_u, the estimated cross-section A_s and the flame surface A_f according to Andrews and Bradley (1972), along with the flame stretching factor K, called Karlovitz factor (Karlovitz et al.,1951). Those parameters were then combined to apply a linear relation linking the burning velocity and the Karlovitz factor K to the laminar burning velocity S_u^0 and the Markstein length δ_M, which is a parameter characterizing the stability of the flame (Clavin, 1985; Markstein, 1964).

2.2 Pressure-time evolution interpretation

In order to take advantage of the standard explosion tests realized in the 20L sphere, some authors such as Silvestrini et al. (2008) developed a correlation between the laminar burning velocity and the parameters P_{max} and K_{St}. Explosions tests were conducted on nanocellulose in the standard 20 L sphere according to international standards (EN 14034-1, 2004; EN 14034-2, 2006), but using chemical igniters of 100 J to avoid an overdriving phenomenon, knowing the minimum ignition energy of the dried nanocellulose is 5 mJ (Santandrea et al., 2019b). Since the values of laminar burning velocity obtained by flame propagation observation are available only at 500 g/m^3, only the results obtained for this concentration are discussed in this work. Nevertheless, tests were performed over a wide range of dust concentration (up to 1250 g/m^3), and the influence of the dust concentration on the laminar burning velocity is discussed by Santandrea et al. (2020). The laminar burning velocity S_u^0 of starch was then calculated from the knowledge of the explosion overpressure P_m and rate of pressure rise $(dP/dt)_m$, using the correlation established by Silvestrini et al. (2008):

$$S_u{}^0 = 0.11 \frac{\left(\frac{dP}{dt}\right)_m V^{1/3}}{P_m \left(\frac{P_m}{P_0}\right)^{0.14} \left(\frac{P_m}{P_0}\right)^{\left(\frac{1}{\gamma}\right)}} \quad (1)$$

where V is the vessel volume, P_0 the atmospheric pressure and γ the ratio of specific heats. This correlation is based on several assumptions, e.g. the flame expansion is spherical, the turbulent length scales are disregarded and the burnt gases remain trapped behind the expanding flame front (Silvestrini et al., 2008).

3. One-dimensional modelling of flame propagation

Complementary to experiments relying on the flame visualization and the pressure-time evolution, the laminar flame velocity was approached using a one-dimension flame propagation model developed by Torrado et al. (2018) and initially designed to describe gas and hybrid mixtures explosions). The model was then adapted to nanocellulose using the same hypothesis than for flame visualization experiments, i.e. considering a fast devolatilization of the dust and a flame propagation kinetically limited by the combustion of the pyrolysis gases. A similar assumption was previously made by several authors, considering that a dust explosion is controlled by homogeneous combustion for diameters lower than 'a critical value' (Eckhoff, 2003; Russo and Di Benedetto, 2013). For instance, based on tests carried out on 110 µm particles, Cashdollar et al. (1989) stated that the explosion of carbonaceous dusts was mainly driven by the gas phase combustion of the volatiles. Di Benedetto and Russo (2007) used this assumption to validate their dust explosion model on 20 µm microcrystalline cellulose. However, it should be clearly stated that this is a strong assumption when dealing with organic microparticles as both the pyrolysis reaction and heat transfer can also control the combustion kinetics. By calculating the values of Biot and Py numbers for cellulose particles, Py being defined as the ratio between the pyrolysis time over the characteristic time for heat transfer (Piskorz et al, 1986), it appears that the heat transfer may control the explosion for particles with diameters greater than 200 µm. For smaller dusts, pyrolysis is certainly the rate-limiting step down to a few micrometers, this 'critical limit' being hard to define as it depends on particles properties. While keeping in mind these limitations and preliminary precautions, the assumption of a fast devolatilization of organic nanopowders was made during the model development.

Moreover, since cellulose and starch are both polymers formed of glucose chains, both compounds are assumed to produce the same pyrolysis gases when tested in the same conditions. It is another strong assumption as the physical properties of the powders (particle size distribution, porosity, shape…) play a significant role in their chemical reactivity.

Pyrolysis experiments were conducted on wheat starch (d_{50} = 22 μm) in a Godbert-Greenwald oven modified according to Dufaud et al. (2012b) to collect the post-pyrolysis gases. Oven temperature was modified over a range of 973 to 1173 K. It should be noted that the minimum ignition temperature (MIT) of cellulose powder is approximately 773K, value depending on the particle size distribution. Due to short residence times, and considering the particle external and internal heat transfers, temperatures lower than 973K will lead to low pyrolysis conversion and to gas amount too low to be analysed correctly. The maximum oven temperature is 1223K and a temperature too different from the MIT would not make it possible to obtain gases representative of those generated during the first phases of ignition (in the preheating zone before their combustion). Therefore, the gas composition obtained for a concentration of approximately 500 g/m^3 and a temperature of 973 K was then used as the initial composition of the fuel (Figure 2) in the model for a numerical determination of the laminar flame velocity of nanocellulose. The mass fraction of the species generated by the pyrolysis of the powder are also given above the bars in Figure 2. It should be emphasized that a different temperature would lead to a different gas composition, especially considering that the carbon dioxide content would decrease and hydrogen and methane concentrations would increase as the temperature rises. Furthermore, such flash-pyrolysis experiments were performed for lean fuel mixtures and the gas composition shown in Figure 2 would not be suitable for fuel rich mixtures (above 750 g/m^3 as stated in 2.1). As a consequence, if the model developed in this work can be very useful to give a first estimate a laminar burning velocity, it would be mistaken to believe that a single composition of pyrolysis gases would be representative of what occurs at every point of the dust cloud and at every moment during a dust explosion.

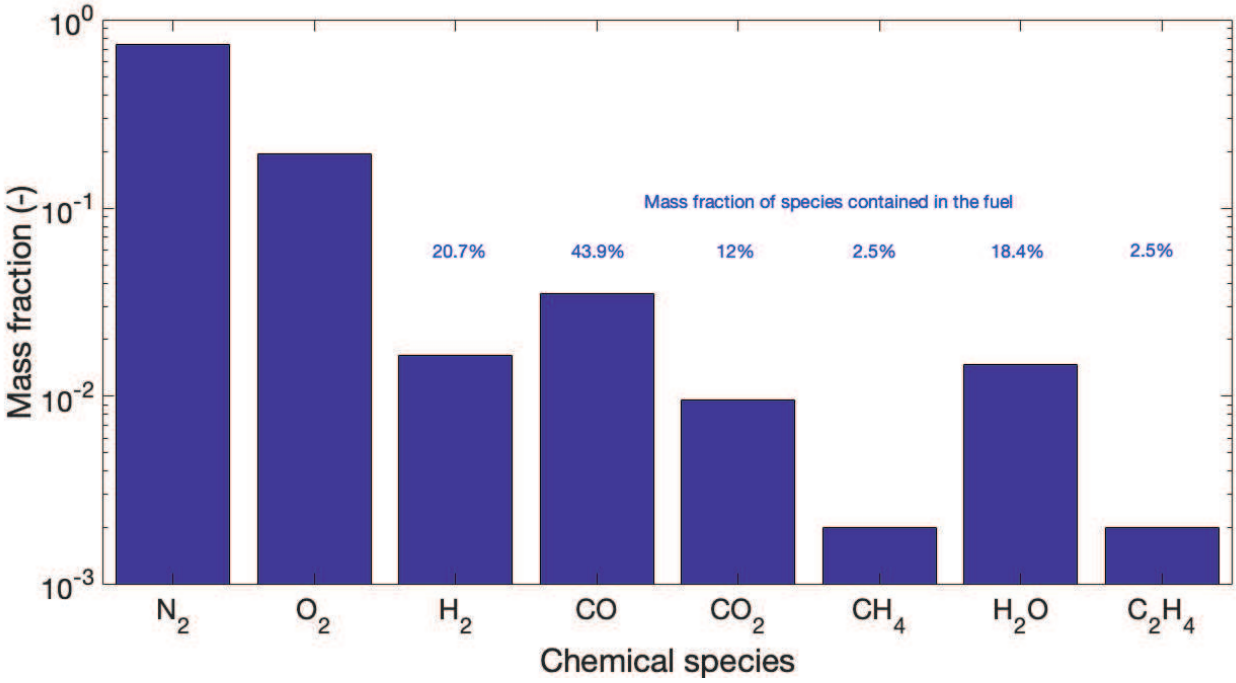

Figure 2. Initial composition of the nanocellulose pyrolysis gases/air mixture considered in the flame propagation model for 500 g/m^3 of nanocellulose

The simulation domain is constituted of a tube with a numerical length of 5 cm involving two parallels walls divided into three distinct zones: preheat, reaction and post-flame, knowing that the flame propagates from the post-flame zone to the preheat zone. Mass, species and energy balances, notably based on the properties of the considered chemical species, were then expressed in the simulation domain. Since the main chemical species constituting the pyrolysis gases of nanocellulose are the same than the species initially considered in the model for the flame propagation of a methane/air flame (Torrado et al., 2018), similar reaction mechanisms were used. However, since the pyrolysis step mainly produced carbon monoxide, a reversible oxidation reaction of this gas to produce carbon dioxide was added (Table 1, reactions 7 and -7). Reactions involving radicals H, OH and O were also considered to improve the prediction of the flame temperature (Frassoldati et al., 2009). The mass reaction rate of a component depends on its molecular weight and the rate of the reactions in which it is involved. The rate of each reaction r_j was then expressed as:

$$r_j = k \prod \varphi^{n_i} \qquad (2)$$

where φ is the mole concentration and n_i the reaction order of the component i in the reaction j. The reaction constant is assumed to follow an Arrhenius law and is defined as:

$$k_j = A_i T^{\beta} \exp\left(\frac{-E_i}{RT}\right) \qquad (3)$$

where A_i is the pre-exponential factor, E_i is the activation energy and β, a temperature exponent.

Table 1: Reaction mechanisms considered for the combustion of the pyrolysis gases (Units in cal, mol, m, s)

#	Reaction	A_i	β	E_i	Reaction order	Reference
1	$CH_4 + 0.5O_2 \rightarrow CO + 2H_2$	2.45×10^9	0	3×10^4	$[CH_4]^{0.5}\,[O_2]^{1.25}$	(Jones and Lindstedt, 1988)
2	$CH_4 + H_2O \rightarrow CO + 3H_2$	3×10^5	0	3×10^4	$[CH_4]\,[H_2O]$	(Jones and Lindstedt, 1988)
3	$CO + H_2O \rightarrow CO_2 + H_2$	2.75×10^6	0	2×10^4	$[CO]\,[H_2O]$	(Jones and Lindstedt, 1988)
-3	$CO_2 + H_2 \rightarrow CO + H_2O$	9×10^7	0	2.8×10^4	$[CO_2]\,[H_2]$	(Torrado et al., 2018)
4	$H_2 + 0.5O_2 \rightarrow H_2O$	3.85×10^{13}	-1	4×10^4	$[H_2]^{0.25}\,[O_2]^{1.50}$	(Jones and Lindstedt, 1988)
-4	$H_2O \rightarrow H_2 + 0.5O_2$	9.27×10^{18}	0.88	9.8×10^4	$[H_2O]\,[H_2]^{-0.75}\,[O_2]$	(Andersen et al., 2009)
5	$O_2 \rightarrow 2O\cdot$	1.5×10^9	0	1.13×10^5	$[O_2]$	(Frassoldati et al., 2009)
6	$H_2O \rightarrow H\cdot + OH\cdot$	2.3×10^{22}	-3	1.2×10^5	$[H_2O]$	(Frassoldati et al., 2009)
7	$CO + 0.5O_2 \rightarrow CO_2$	1.26×10^4	0	10×10^3	$[CO]\,[O_2]^{0.25}\,[H_2O]^{0.5}$	(Andersen et al., 2009)

-7	$CO_2 \rightarrow CO + 0.5O_2$	1.95×10^{12}	-0.97	78.4×10^3	$[CO_2]\,[H_2O]^{0.5}\,[O_2]^{-0.25}$	(Andersen et al., 2009)

196

197 The calculation of the flame velocity then relies on the numerical integration of the differential
198 equations of mass, species and energy:

199 $$\frac{\partial \rho}{\partial t} + div(\rho u) = 0 \quad (4)$$

200 $$\frac{\partial}{\partial t}(\rho y_i) + div(\rho y_i u) + div(j_i) = \dot{\omega}_i \quad (5)$$

201 where j_i, ρ, y_i and u are respectively the mass diffusion flux, the mixture density, the mass fraction
202 of the i^{th} component, and the velocity. The reaction rate of the component i, depends on the molecular
203 weight W_i and on the stoichiometric coefficient of the component i in the reaction j:

204 $$\dot{\omega}_i = W_i \sum_{j=1}^{N_r} v_{i,j} r_j \quad (6)$$

205 The energy balance is developed as follows, assuming a constant pressure and negligible viscous
206 forces (Torrado et al., 2018):

207 $$\sum_{i=1}^{N} C_{p,i}[\rho y_i \partial_t(T) + \rho y_i u div(T) + j_i div(T)] = -\dot{\omega}_i\left[\sum_{i=1}^{Nspecies}\left[h_{f,i}^0 + C_{p,i}T\right]\right] +$$

208 $$div(\lambda \nabla \mathrm{T}) + Q_{rad} \quad (7)$$

209 The radiation term Q_{rad} will be developed in section 4.2.

210 The space derivatives were discretized using the finite volume method with 160 control volumes to
211 obtain a system of ordinary differential equations, which was solved using the integration functions
212 ODE (ordinary differential equations) in Matlab. A mesh independence study was carry out by
213 beginning with 40 control volumes and increasing progressively the mesh resolution by 1.2. The
214 expression of the mass and species balance, the mass diffusion fluxes and the energy balance, along
215 with the numerical resolution, are properly described by Torrado et al. (2018).

216 The resolution of the ordinary differential equations requires an initial value of the temperature and
217 mass fractions of all the considered species in every numerical domain. The composition in the
218 preheat zone, which represents 25% of the numerical domain, is defined by the mass fractions of the
219 considered mixture in laboratory conditions. As a first approximation, the mass fractions and

temperature are assumed to evolve linearly in the reaction zone, implying those values are known if the initial and final conditions are fixed. To estimate the conditions in the post-flame zone (70% of the considered distance), the adiabatic temperature and mass fraction of the burnt gases for a steady flame were calculated using PREMIX program (Kee et al., 1993). This approach, represented in Figure 3, was used to reduce the calculation time and to improve the convergence of the program, by initializing all the conditions close to a stable solution. Since this numerical model also aims at considering the radiative heat transfer induced by the presence of nanoparticles in the mixture, which is not the case of the PREMIX program, this latter was not considered as a suitable method to determine the laminar burning velocity of nanopowders.

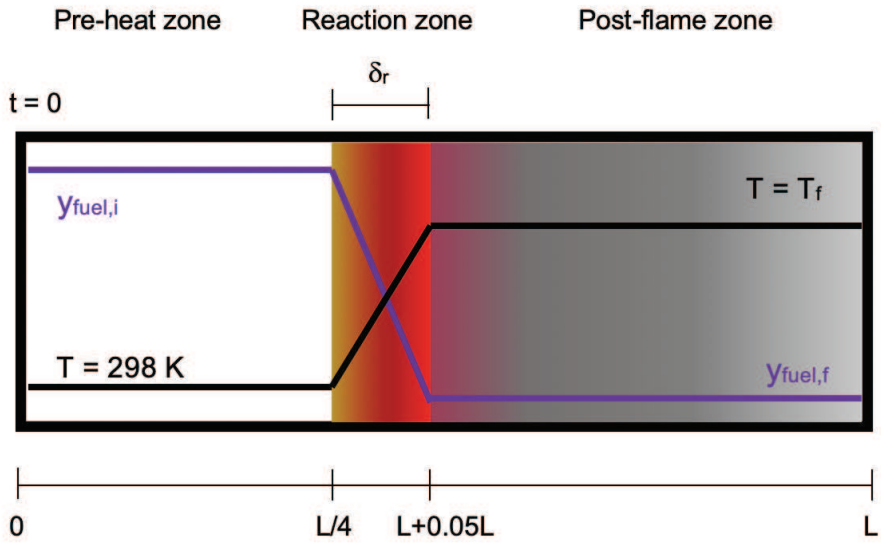

Figure 3. Schema of the initial conditions of the temperature and fuel fraction in each zone of the flame

The system previously defined was then analyzed considering a distance L of 5 cm and an integration time of 50 ms. In order to show an example of raw results obtained by a simulation, the evolution of the temperature with time is presented in Figure 4 for an initial fuel concentration of 500 g/m^3. The different positions indicated in Figure 4 correspond to various zones: i) the temperature evolution in the preheat zone is represented by the curves at 0.66 and 0.91 cm, ii) the flame boundaries are located at 1.22 cm and 1.45 cm (including 1.25 cm), and iii) the time-evolution of the temperature in the post-

flame zone is given at 5 cm. It appears that, in the post-flame zone (5 cm), the temperature is constant with time, since the reaction already occurred. Then, a fast increase of the temperature after a few milliseconds is visible in the reaction zone, especially at 1.22 and 1.25 cm. The thermal wave progressively shifts toward the preheat zone with time, describing the propagation of the flame.

The 1D model was previously validated on methane/air mixtures (Torrado et al., 2018) as it gives a laminar burning velocity of 34 cm/s, which is close to the experimental values of methane/air burning velocity from 34 to 38 cm/s (Dirrenberger et al., 2011; Proust, 2006). Moreover, the model shows a good agreement with commercial software (PREMIX program) to estimate the mass fraction of burnt gases and the final temperature; for instance, the flame temperature of a stoichiometric CH_4/air mixture obtained by the 1D model is 2271 K compared to a theoretical adiabatic temperature of 2236 K.

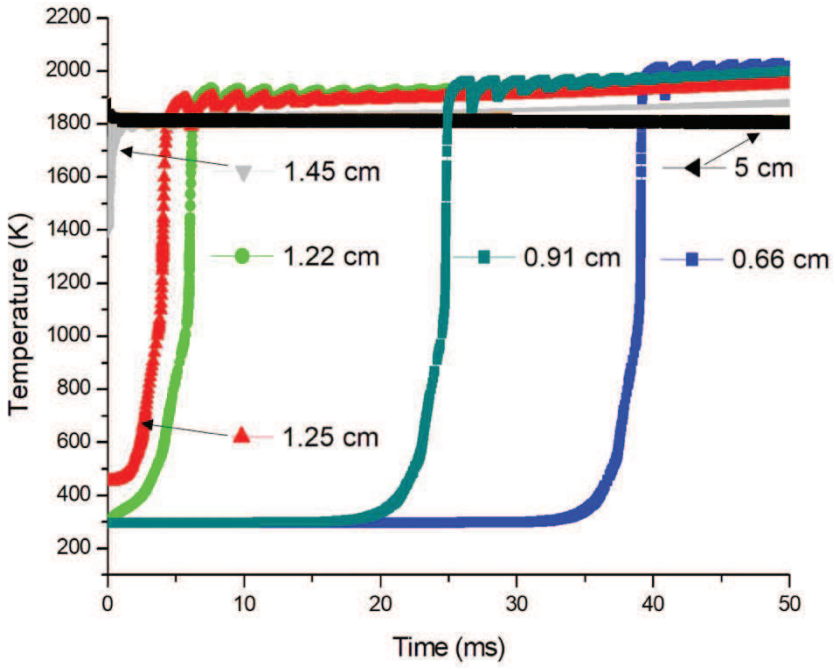

Figure 4. Evolution of the temperature with time for different control volumes when modelling the flame propagation of nanocellulose (quiescent conditions, dust concentration : 500 g/m^3)

4. Results and discussion

4.1 Combustion of the pyrolysis gases

The position of the flame front, assimilated to the position of the highest temperature, was recorded for each integration time and is presented in Figure 4. It should be reminded that the reaction zone was initially located between 1.25 cm and 1.5 cm. However, before 1 ms, a very fast displacement of the flame is observed, preventing a clear determination of the flame front position between 1.4 and 1.5 cm. Nevertheless, a linear evolution of the flame position with time can be observed from 1 ms to 50 ms. A laminar flame velocity of 17.5 cm/s, represented by the slope of the linear regression, was then obtained for the combustion of nanocellulose. It should be stressed that this value should be viewed with caution as the pyrolysis step has been considered as very fast with regard to the combustion of the pyrolysis gases, which is a strong assumption only validated form very small particles.

The flame velocity calculated using the flame propagation model was then compared to the values experimentally obtained by Santandrea et al. (2020) (Table 2). The value determined numerically appears to be of the same order of magnitude than the experimental ones (from 16.9 to 23.5 cm/s), with a maximum difference of 22% with regard to the laminar flame velocity measured in the flame propagation tube. This value is also consistent with laminar flame velocity of "wood gas" at the stoichiometry mentioned in the literature by Mollenhauer and Tschöke (2010) and Przybyla et al. (2008), reaching around 14 cm/s and 20 cm/s respectively. Moreover, these results are also in agreement with the flame velocities of dusts, i.e. from 15 to 30 cm/s for the unstretched laminar burning velocity of cornstarch (Dahoe et al., 2002) and from 15 to 55 cm/s, proposed by Sattar et al. (2014) for various powders such as lycopodium, coal and walnut shells. Nevertheless, the difference between experimental and numerical values can obviously come from experimental uncertainties, but can also be due to the omission of both the contribution of the radiative heat transfer to the flame propagation or of the pyrolysis reaction. Indeed, if the pyrolysis step can decrease the flame velocity due to a kinetic limitation, the fresh or unburnt remaining particles can also improve the flame propagation through a heat transfer modification in the preheat zone. Such impacts on the radiative transfers and on the flame speed were notably observed in the visible spectrum when combustible or

even inert particles (carbon black or alumina) were added to methane (Torrado et al., 2017). To numerically evaluate this influence, the contribution of the radiative heat transfer, added to the flame propagation model by Torrado et al. (2018) and based on the work of Haghiri and Bidabadi (2010), will be now considered during the combustion of the pyrolysis gases of nanocellulose.

Table 2: Numerical and experimental values of laminar flame velocity of nanocellulose

Determination method	Laminar flame velocity (cm/s)
Flame propagation model	17.5
Flame visualization: propagation tube	21.4 ± 1
Flame visualization: vented sphere	20.5 ± 3
20L sphere: application of Silvestrini et al. (2008) correlation	19.9 ± 3

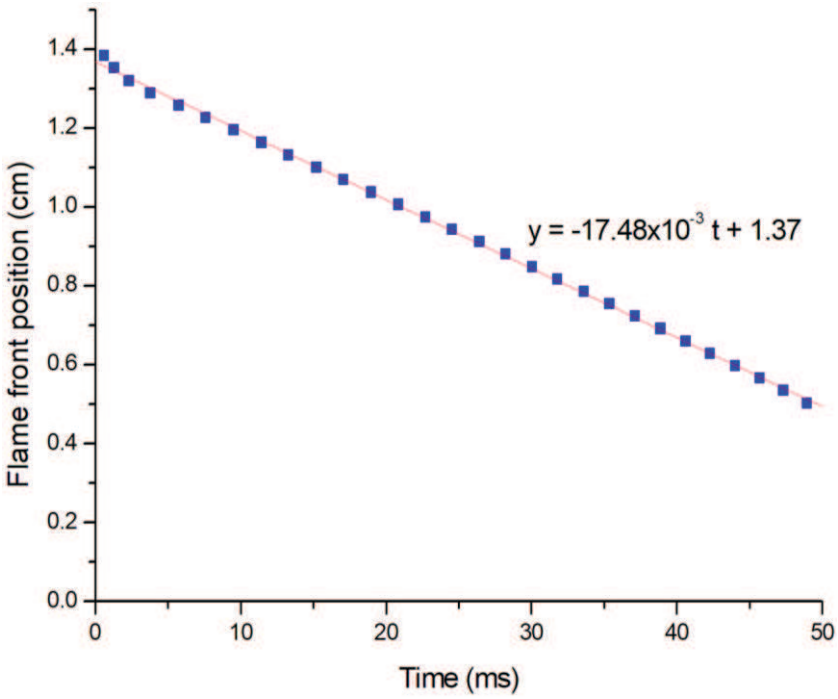

Figure 4. Evolution of the flame front position with time during the combustion of nanocellulose pyrolysis gases

4.2 Influence of the radiative heat transfer

Since the pyrolysis of nanocellulose particles and the combustion of the pyrolysis gases happen simultaneously, the unburnt particles can impact the flame propagation by variations of the heat transfer. However, the remaining dust can hardly be quantified and characterized for each integration time without taking the pyrolysis kinetics into account. Thus, several dust concentrations, assumed constant with time, were tested. The dust clouds were supposed to be homogeneous over the simulation domain and constituted of monodispersed spherical particles. Moreover, due to the agglomeration of the nanoparticles, the particle size after dispersion must be considered (Santandrea et al., 2019a). As described in section 2.1, particle size distribution measurements after dispersion of nanocellulose in the 20L sphere led to a mean value of 10 µm (Santandrea et al., 2020). This value was then chosen as a reference for the calculation, along with 100 nm, to represent the primary particles, and 60 µm, which is the mean diameter of nanocellulose agglomerates before dispersion, i.e. the agglomerates not broken by the dispersion process. In this model, Mie scattering, valid for micron particles, was then used to define the radiative heat transfer. It should be noted that Rayleigh scattering, encountered for particles smaller than 100 nm, do not contribute significantly to the flame expansion due to the emission in every direction (Hong and Winter, 2006). Thus, decreasing the particle size below this size would only decrease the radiative heat transfer contributing to the flame propagation, and so the flame velocity. The concentration of dust that did not react during the combustion of the 500 g/m^3 of nanocellulose was varied from 2.5 g/m^3 to 100 g/m^3. These values were chosen as orders of magnitude to represent the radiative heat transfer at the beginning and at the end of the reaction. The radiative heat transfer was then added to the energy balance, and the heat capacity of the dust was then taken into account during the calculation of the mean heat capacity of the mixture. Due to the assumption of a fast pyrolysis, the heterogeneous reactions involving the solid particles were not considered in the model. However, it should be noted that Torrado et al. (2018) evidenced that the contribution of the chemical reactions of the powder is negligible with regard to the contribution of the radiative heat transfer at low concentrations (2.5 g/m^3).

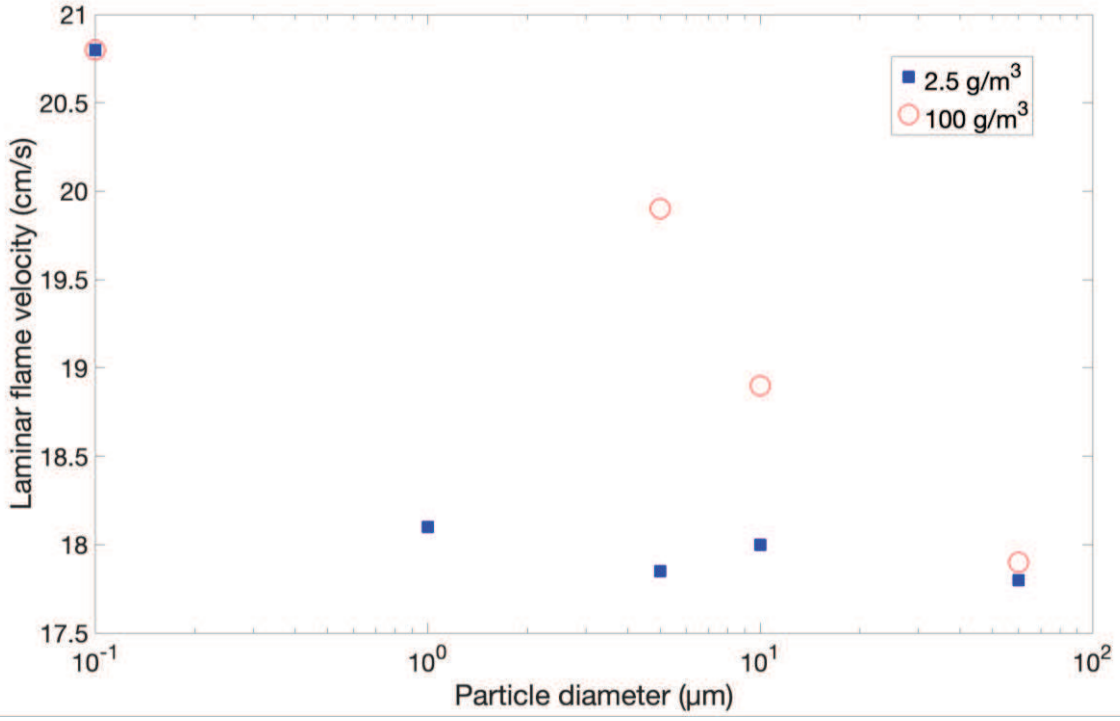

Figure 6. Numerical values of the laminar flame velocity of a mixture of nanocellulose pyrolysis gases (500 g/m^3) and inert particles considered for the radiative heat transfer: influence of the inert particle diameter at 2.5 and 100 g/m^3.

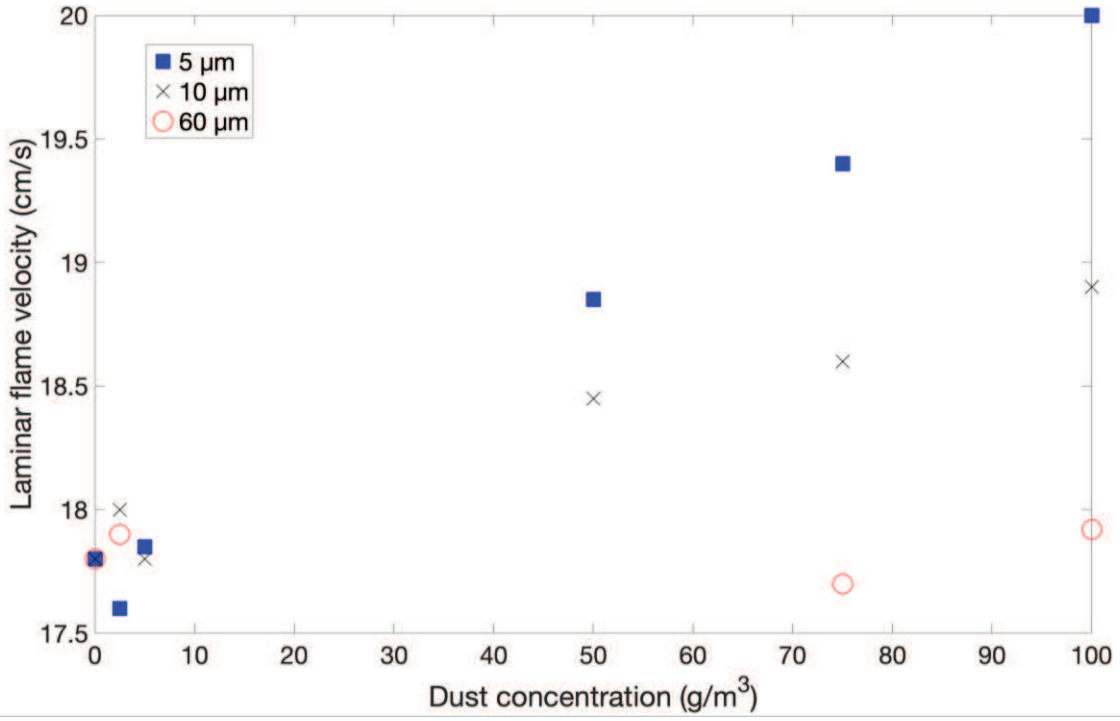

Figure 7. Numerical values of the laminar flame velocity of a mixture of nanocellulose pyrolysis gases (500 g/m^3) and inert particles considered for the radiative heat transfer: influence of the inert powder concentration for particle diameters of 5, 10 and 60 µm.

Figure 6 confirms that the laminar flame velocity obviously varies as a function of the particle size distribution (Ghaffari et al., 2019) and of the dust concentration. In Figure 6, it also appears that small particles contribute more to the radiative heat transfer than bigger particles in the micro-range. Indeed, particles of 60 µm bring similar contribution to the flame acceleration, i.e. around 0.5 cm/s, at 2.5 g/m^3 and 100 g/m^3, whereas 100 g/m^3 of 5 µm particles lead to a flame velocity of 20 cm/s, i.e. 14% higher than the flame velocity of the pyrolysis gases. At this point, it should be stressed that for large particles, the assumption of a fast pyrolysis with regard to the combustion reaction is certainly not valid and that simulations presented for powders having a mean diameter larger than 10 µm are only given as an indication. It should also be underlined that the contribution of particles of 100 nm to the radiative heat transfer may be overestimated since Mie scattering was considered for the calculation whereas Rayleigh scattering is more representative of the heat transfer of nanoparticles. In Figure 7, it appears that a dust concentration of 2.5 g/m^3 leads to a mean flame velocity of around 17.8 cm/s for particles between 5 and 60 µm. Therefore, increasing the concentration also increases the contribution of the radiative heat transfer to the flame propagation, reaching 20.0 cm/s when considering 100 g/m^3 of particles of 5 µm.

Both the dust concentration and the particle size are thus of great importance when considering the radiative heat transfer. As proposed by various authors (Haghiri and Bidabadi, 2010; Meinköhn et al., 2007), the absorbed, emitted and scattered energy in a dust cloud can be expressed as:

$$\frac{dI}{dx} = K_a I + K_s I - K_a I_b - \frac{K_s}{4\pi}\int_{4\pi} I(\Omega) P d\Omega \qquad (8)$$

where I and I_b are the thermal intensity and thermal intensity of a black body. An analytical solution of equation 8 was proposed by Haghiri and Bidabadi (2010) for each zone represented in Figure 3. By neglecting the multi-scattering contribution, i.e. for isotropic scattering, the integral term can be removed from equation 8. The absorption coefficient K_a and the scattering coefficient K_s directly depend on the dust concentration, the dust density and the particle size, as follows (Haghiri and Bidabadi, 2010):

$$K_a = \frac{3}{2}\frac{C}{\rho_p\, d_p}\, Q_{abs} \quad (9)$$

$$K_s = \frac{3}{2}\frac{C}{\rho_p\, d_p}\, Q_{sca} \quad (10)$$

where C is the dust concentration, ρ_p the particle density, d_p the particle diameter and $Q_{abs} = \varepsilon_P$ and $Q_{sca} = 1- \varepsilon_P$ respectively the absorption and scattering efficiency, and particle emissivity ε_P. In the preheat zone, only the absorption term was considered, whereas both absorption and scattering were considered in the reaction and post-flame zones. The implementation of both equations (9) and (10) in the 1D model was detailed by Torrado et al. (2008). The thermal properties of cellulose powders were considered as inputs.

The absorption and scattering coefficients are then directly proportional to the total surface area (TSA) developed by the particles in the cloud, which can be expressed as follows for spherical particles:

$$TSA = \frac{6\, C}{\rho_p\, d_p} \quad (11)$$

Once again, simulations were performed by considering the combustion of pyrolysis gases representative of the devolatilization of nanocellulose (Figure 2) and at an initial mass concentration of 500 g/m^3. In order to consider the radiative contribution of the powder on the flame propagation, particles having the same thermal properties than cellulose were numerically added to the reactive system; however, potential heterogeneous reactions were not taken into account. A linear evolution of the calculated flame velocity with the total surface area developed by the particles considered in the radiative heat transfer appears in Figure 8. It can be observed that the radiative heat transfer generated by particles developing a total surface area lower than 10 m^2/m^3 does not lead to a significant increase of the flame velocity, with values between 17.5 and 18 cm/s. However, when considering a total surface area of 100 m^2/m^3, a flame velocity of 20.8 cm/s is reached, thus proving the importance of considering the surface area when analysing dust explosions, instead of focusing only on mass concentration. It should also be noted that increasing the concentration too much would

lead to an important increase of absorption, which would hence limit the heat radiation in the preheat zone.

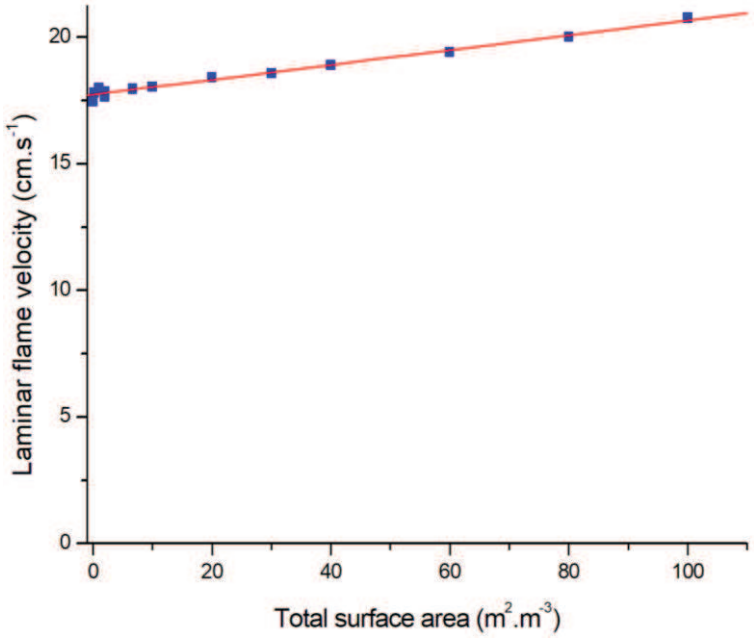

Figure 8. Influence of the total surface area of the particles implied in the radiative heat transfer on the flame velocity of a mixture of nanocellulose pyrolysis gases (500 g/m^3) and inert particles

5. Conclusions

The laminar burning velocity of nanocellulose has been determined using a one-dimensional flame propagation model adapted from a model already validated for hybrid mixtures. The numerical system, composed of mass and energy balances equations and of mass reaction rates adapted to the combustion reactions, was solved by the finite volume method. Assuming that the devolatilization of organic nanopowders is fast, the chemical reactions were considered limited to the combustion of the pyrolysis gases. A first value of laminar flame velocity of 17.5 cm/s was obtained for 500 g/m^3 of nanocellulose, which is close to values experimentally measured in a flame propagation tube or a 20 L sphere, around 21 cm/s, thus showing a good consistency between the numerical and experimental approaches.

However, since in practice, the devolatilization of the particles is not instantaneous, the remaining particles can contribute to the radiative heat transfer, which was added to energy balance. Due to the tendency of nanoparticles to agglomerate, different particle diameters and dust concentrations were tested. Thus, although the heat transfer of nanoparticles tends to be neglected due to Rayleigh scattering, which does not contribute to the flame propagation, the contribution of the remaining micro-agglomerates after dispersion must be considered. Indeed, the existence of a linear relation between the laminar flame velocity and the total surface area developed by the particles implied in the radiative heat transfer was highlighted. A flame velocity reaching 20.8 cm/s for a total surface area of 100 m^2/m^3 considered for the radiative heat transfer was then obtained, showing a strong impact of the heat radiation on the flame propagation.

Nevertheless, it should be kept in mind that, even if the nanocellulose pyrolysis could be considered as very fast, this assumption is potentially not valid for nanopowders agglomerates and certainly not for larger organic particles. In the latter case, consideration of the pyrolysis kinetics, using for instance a semi-global lumped-reaction system, will be necessary. In any case, this work shows that knowledge of the kinetics of pyrolysis and/or combustion allows the numerical assessment of a laminar flame velocity, provided that the radiative phenomena are also taken into consideration.

Acknowledgements

This work was supported financially by the French Ministry for the Ecological and Solidary Transition and The French Ministry for Higher Education and Research.

References

Amyotte, P.R., Chippett, S., Pegg, M.J., 1988. Effects of turbulence on dust explosions. Prog. Energy Combust. Sci. 14, 293–310. https://doi.org/10.1016/0360-1285(88)90016-0

418 Andersen, J., Rasmussen, C.L., Giselsson, T., Glarborg, P., 2009. Global Combustion Mechanisms
419 for Use in CFD Modeling under Oxy-Fuel Conditions. Energy & Fuels 23, 1379–1389.
420 https://doi.org/10.1021/ef8003619
421 Andrews, G.E., Bradley, D., 1972. Determination of burning velocities: A critical review.
422 Combustion and Flame 18, 133–153. https://doi.org/10.1016/S0010-2180(72)80234-7
423 Belerrajoul, M., 2019. Modélisation multi-échelle de la combustion d'un nuage de particules (PhD
424 Thesis). National Polytechnic Institute of Toulouse.
425 Boilard, S.P., Amyotte, P.R., Khan, F.I., Dastidar, A.G., Eckhoff, R.K., 2013. Explosibility of
426 micron- and nano-size titanium powders. J. Loss Prev. Process Ind. 26, 1646–1654.
427 https://doi.org/10.1016/j.jlp.2013.06.003
428 Bouillard, J., Vignes, A., Dufaud, O., Perrin, L., Thomas, D., 2010. Ignition and explosion risks of
429 nanopowders. Journal of Hazardous Materials 181, 873–880.
430 https://doi.org/10.1016/j.jhazmat.2010.05.094
431 Bradley, D., Lee, J.H.S., 1984. . Proceedings of the first international colloquium on the explosibility
432 of industrial dusts 220–223.
433 Cashdollar, K.L., Hertzberg, M., Zlochower, I.A., 1989. Effect of volatility on dust flammability
434 limits for coals, gilsonite, and polyethylene, Symposium (International) on Combustion, 22,
435 1, 1757-1765.
436 Clavin, P., 1985. Dynamic behavior of premixed flame fronts in laminar and turbulent flows. Progress
437 in Energy and Combustion Science 11, 1–59. https://doi.org/10.1016/0360-1285(85)90012-7
438 Cuervo, N., 2015. Influences of turbulence and combustion regimes on explosions of gas-dust hydrid
439 mixtures (PhD Thesis). The University of Lorraine, France.
440 Cuervo, N., Dufaud, O., Perrin, L. Determination of the burning velocity of gas/dust hybrid mixtures
441 (2017) Process Saf. Environ., 109, pp. 704-715. https://doi.org/10.1016/j.psep.2017.06.009

442 Dahoe, A.E., Cant, R.S., Scarlett, B., 2001. On the Decay of Turbulence in the 20-Liter Explosion
443 Sphere. Flow, Turbulence and Combustion 67, 159–184.
444 https://doi.org/10.1023/A:1015099110942
445 Dahoe, A.E., Hanjalic, K., Scarlett, B., 2002. Determination of the laminar burning velocity and the
446 Markstein length of powder–air flames. Powder Tech., Special issue in Honour of Prof Jimbo
447 122, 222–238. https://doi.org/10.1016/S0032-5910(01)00419-3
448 Di Benedetto, A., Russo, P., 2007. Thermo-kinetic modelling of dust explosions. J. Loss Prev. Process
449 Ind., Selected Papers Presented at the Sixth International Symposium on Hazards, Prevention
450 and Mitigation of Industrial Explosions 20, 303–309.
451 https://doi.org/10.1016/j.jlp.2007.04.001
452 Di Benedetto, A., Russo, P., Amyotte, P., Marchand, N., 2010. Modelling the effect of particle size
453 on dust explosions (2010) Chemical Engineering Science, 65 (2), pp. 772-779.
454 https://doi.org/10.1016/j.ces.2009.09.029

455 Dirrenberger, P., Le Gall, H., Bounaceur, R., Herbinet, O., Glaude, P.-A., Konnov, A., Battin-
456 Leclerc, F., 2011. Measurements of Laminar Flame Velocity for Components of Natural Gas.
457 Energy Fuels 25, 3875–3884.

458 Dufaud, O., Khalili, I., Cuervo-Rodriguez, N., Olcese, R.N., Dufour, A., Perrin, L., Laurent, A.,
459 2012a. Highlighting the Importance of the Pyrolysis Step on Dusts Explosions. Chemical
460 Engineering Transactions 26, 369–374.
461 Dufaud, O., Poupeau, M., Khalili, I., Cuervo, N., Christodoulou, M., Olcese, R., Dufour, A., Perrin,
462 L., 2012b. Comparing Pyrolysis Gases and Dusts Explosivities: A Clue to Understanding
463 Hybrid Mixtures Explosions? Ind. Eng. Chem. Res. 51, 7656–7662.
464 https://doi.org/10.1021/ie201646s
465 Dufaud, O., Vignes, A., Henry, F., Perrin, L., Bouillard, J., 2011. Ignition and explosion of
466 nanopowders: something new under the dust. Journal of Physics: Conference Series 304,
467 012076. https://doi.org/10.1088/1742-6596/304/1/012076

Eckhoff, R.K., 2003. Dust Explosions in the Process Industries - 3rd Edition, 3rd ed. Gulf Professional Publishing.

EN 14034-1, 2004. Determination of explosion characteristics of dust clouds — Part 1: Determination of the maximum explosion pressure P_{max} of dust clouds.

EN 14034-2, 2006. Determination of explosion characteristics of dust clouds — Part 2: Determination of the maximum rate of explosion pressure rise (dp/dt)max of dust clouds.

Fauske, H.K., Clouthier, M.P., 2015. A theoretical-based and generalized method for dust and gaseous deflagration Vent sizing. 49th Annual Loss Prevention Symposium 2015, LPS 2015 - Topical Conference at the 2015 AIChE Spring Meeting and 11th Global Congress on Process Safety, 573-581.

Frassoldati, A., Cuoci, A., Faravelli, T., Ranzi, E., Candusso, C., Tolazzi, D., 2009. Simplified kinetic schemes for oxy-fuel combustion. 1st International Conference on Sustainable Fossil Fuels for Future Energy – S4FE 2009.

Ghaffari, M., Hoffmann, A.C., Skjold, T., Eckhoff, R.K., van Wingerden, K., 2019. A brief review on the effect of particle size on the laminar burning velocity of flammable dust: Application in a large-scale CFD tool. J. Loss Prev. Process Ind., 62, art. no.103929. https://doi.org/10.1016/j.jlp.2019.103929

Haghiri, A., Bidabadi, M., 2010. Modeling of laminar flame propagation through organic dust cloud with thermal radiation effect. International Journal of Thermal Sciences 49, 1446–1456. https://doi.org/10.1016/j.ijthermalsci.2010.03.013

Hong, S.-H., Winter, J., 2006. Size dependence of optical properties and internal structure of plasma grown carbonaceous nanoparticles studied by in situ Rayleigh-Mie scattering ellipsometry. Journal of Applied Physics 100, 064303. https://doi.org/10.1063/1.2338132

Jones, W.P., Lindstedt, R.P., 1988. Global reaction schemes for hydrocarbon combustion. Combustion and Flame 73, 233–249. https://doi.org/10.1016/0010-2180(88)90021-1

493 Karlovitz, B., Denniston, D.W., Wells, F.E., 1951. Investigation of Turbulent Flames. J. Chem. Phys.
494 19, 541–547. https://doi.org/10.1063/1.1748289
495 Kee, R.J., Grcar, J.F., Smooke, M.D., Miller, J.A., Meeks, E., 1993. PREMIX: A Fortran program
496 for modeling steady laminar one-dimensional premixed flames.
497 Krietsch, A., Scheid, M., Schmidt, M., Krause, U., 2015. Explosion behaviour of metallic nano
498 powders. J. Loss Prev. Process Ind. 36, 237–243. https://doi.org/10.1016/j.jlp.2015.03.016
499 Markstein, G.H., 1964. Non-steady flame Propagation. P22, Pergarmon, New York.
500 Meinköhn, E., Kanschat, G., Rannacher, R., Wehrse, R., 2007. Numerical methods for
501 multidimensional radiative transfer, in: Reactive Flows, Diffusion and Transport. Springer,
502 pp. 485–526.
503 Mollenhauer, K., Tschöke, H., 2010. Handbook of Diesel Engines. Springer Science & Business
504 Media.
505 Murillo, C., Amín, M., Bardin-Monnier, N., Muñoz, F., Pinilla, A., Ratkovich, N., Torrado, D.,
506 Vizcaya, D., Dufaud, O., 2018. Proposal of a new injection nozzle to improve the
507 experimental reproducibility of dust explosion tests. Powder Tech. 328, 54–74.
508 https://doi.org/10.1016/j.powtec.2017.12.096
509 Piskorz, D., Radlein, A., Scott, D.S., 1986. On the mechanism of the rapid pyrolysis of cellulose,
510 Journal of Analytical and Applied Pyrolysis, 121-137.
511 Proust, C., 2006. Flame propagation and combustion in some dust-air mixtures. J. Loss Prev. Process
512 Ind. 19, 89–100.
513 Przybyla, G., Ziolkowski, L., Szlęk, A., 2008. Performance of SI engine fuelled with LCV gas.
514 Poland: Institute of Thermal Technology.
515 Russo, P., Di Benedetto, A., 2013. Review of a dust explosion modelling, Chemical Engineering
516 Transactions, 31,955-960.

517 Santandrea, A., Gavard, M., Pacault, S., Vignes, A., Perrin, L., Dufaud, O., 2020. 'Knock on
518 nanocellulose': Approaching the laminar burning velocity of powder-air flames. Process Saf.
519 Environ. 134, 247–259. https://doi.org/10.1016/j.psep.2019.12.018
520 Santandrea, A., Pacault, S., Perrin, L., Vignes, A., Dufaud, O., 2019a. Nanopowders explosion:
521 Influence of the dispersion characteristics. J. Loss Prev. Process Ind. 62, 103942.
522 https://doi.org/10.1016/j.jlp.2019.103942
523 Santandrea, A., Vignes, A., Krietsch, A., Perrin, L., Laurent, A., Dufaud, O., 2019b. Some Key
524 Considerations when Evaluating Explosion Severity of Nanopowders. Chem. Eng. T. 77,
525 235–240. https://doi.org/10.3303/CET1977040
526 Sattar, H., Andrews, G.E., Phylaktou, H.N., Gibbs, B.M., 2014. Turbulent flames speeds and laminar
527 burning velocities of dusts using the ISO 1 m3 dust explosion method. Ch. Eng. Trans., 36,
528 157-162. https://doi.org/10.3303/CET1436027.
529 Silvestrini, M., Genova, B., Leon Trujillo, F.J., 2008. Correlations for flame speed and explosion
530 overpressure of dust clouds inside industrial enclosures. J. Loss Prev. Process Ind. 21, 374–
531 392. https://doi.org/10.1016/j.jlp.2008.01.004
532 Skjold, T., 2003. Selected aspects of turbulence and combustion in 20-Litre explosion vessel (Master
533 thesis). University of Bergen, Norway.
534 Torrado, D., Cuervo, N., Pacault, S., Glaude, P.-A., Dufaud, O., 2017. Influence of carbon black
535 nanoparticles on the front flame velocity of methane/air explosions. J. Loss Prev. Process Ind.,
536 49, pp. 919-928. https://doi.org/10.1016/j.jlp.2017.02.006
537 Torrado, D., Pinilla, A., Amin, M., Murillo, C., Munoz, F., Glaude, P.-A., Dufaud, O., 2018.
538 Numerical study of the influence of particle reaction and radiative heat transfer on the flame
539 velocity of gas/nanoparticles hybrid mixtures. Process Saf. Environ. 118, 211–226.
540 https://doi.org/10.1016/j.psep.2018.06.042
541 Traoré, M., Dufaud, O., Perrin, L., Chazelet, S., Thomas, D., 2009. Dust explosions: How should the
542 influence of humidity be taken into account? Process Saf. Environ., 12th International

543 Symposium of Loss Prevention and Safety Promotion in the Process Industries 87, 14–20.
544 https://doi.org/10.1016/j.psep.2008.08.001
545 Yao, N., Wang, L., Bai, C., Liu, N., Zhang, B., 2020. Analysis of dispersion behavior of aluminum
546 powder in a 20 L chamber with two symmetric nozzles. Process Safety Progress 39.
547 https://doi.org/10.1002/prs.12097
548 Zalosh, R., 2019. Dust explosions: Regulations, standards, and guidelines, in: Methods in Chemical
549 Process Safety. Elsevier, pp. 229–282. https://doi.org/10.1016/bs.mcps.2019.03.003
550 Zhen, G., Leuckel, W., 1997. Effects of ignitors and turbulence on dust explosions. J. Loss Prev.
551 Process Ind. 10, 317–324. https://doi.org/10.1016/S0950-4230(97)00021-1
552

Figure1

Nanocellulose explosions
500 g.m^{-3} – tv > 300 ms

4000 fps

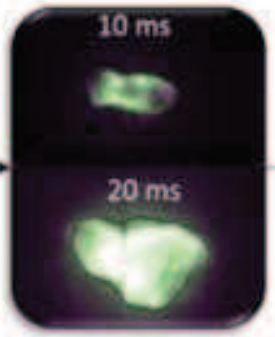

Video analysis – flame kernel growth
Matlab's Simulink – Vision toolbox

$$S_u = S_s \frac{A_s}{A_f}$$

$$K = \frac{1}{A_f}\frac{dA_f}{dt}$$

$$S_u = -\delta_M K + S_u{}^0$$

Figure2

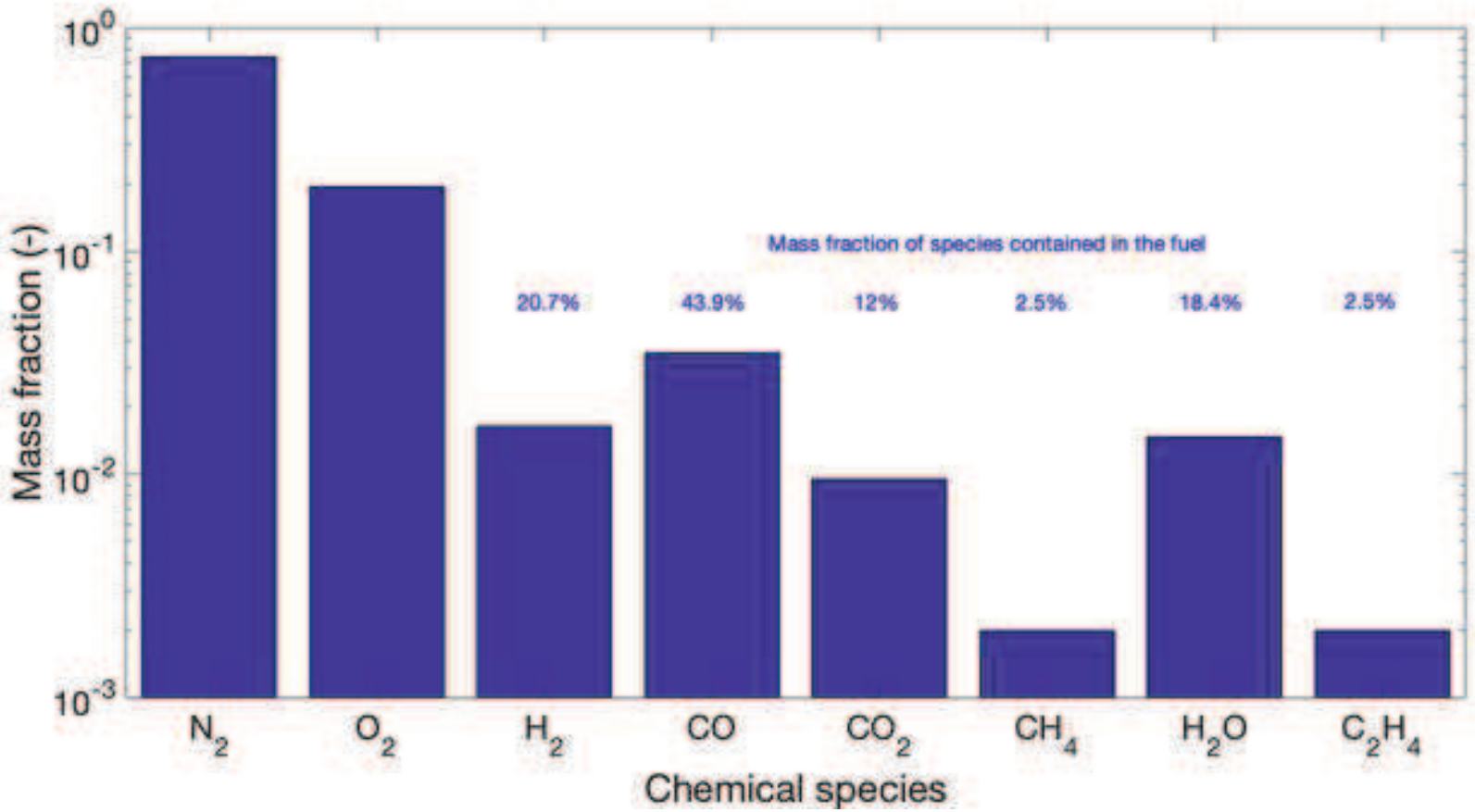
Mass fraction (-)
10^{0}
10^{-1}
10^{-2}
10^{-3}
Mass fraction of species contained in the fuel
20.7%
43.9%
12%
2.5%
18.4%
2.5%
N_2
O_2
H_2
CO
CO_2
CH_4
H_2O
C_2H_4
Chemical species

Figure3

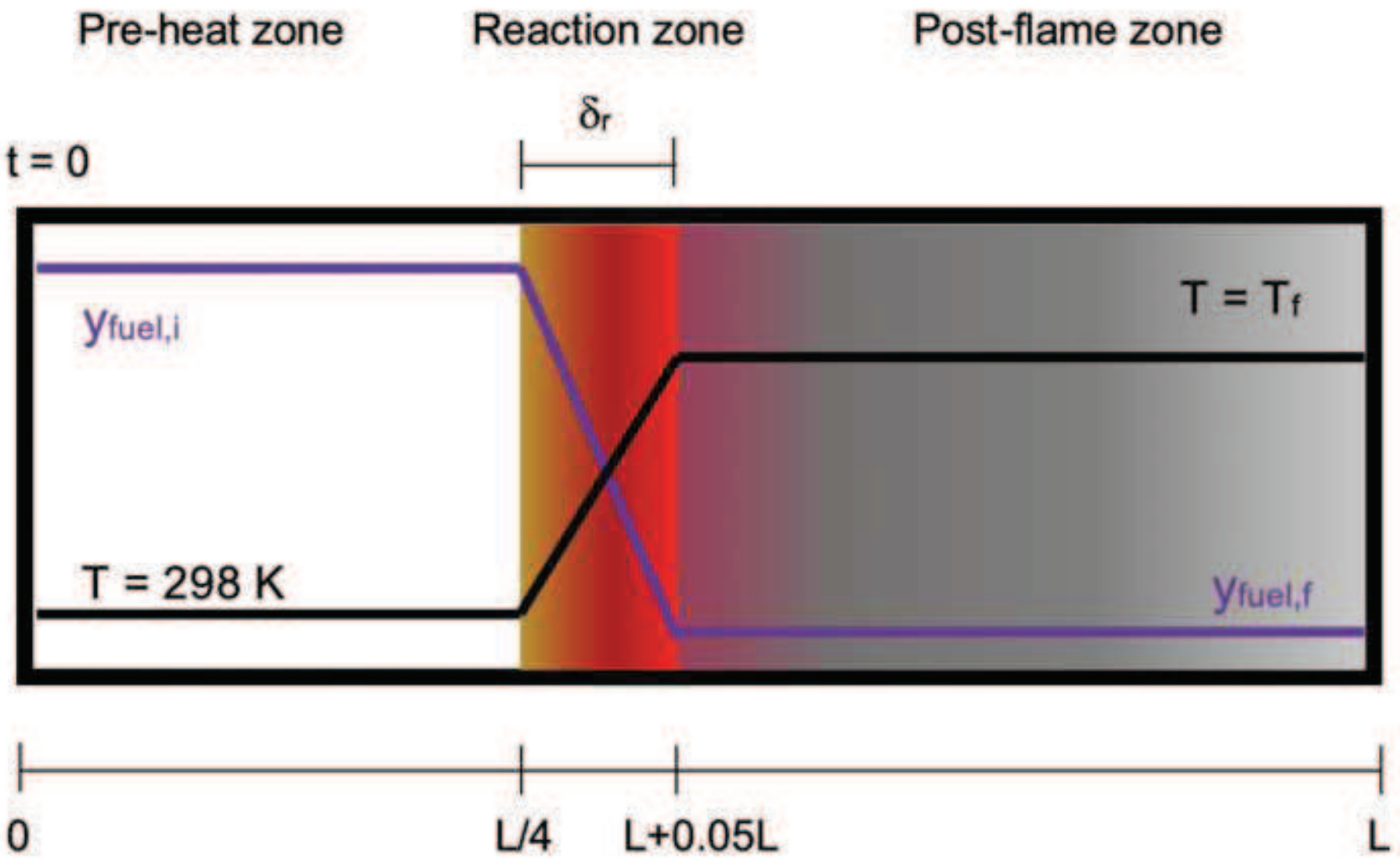
Pre-heat zone
Reaction zone
Post-flame zone
δr
t = 0
yfuel,i
T = Tf
T = 298 K
yfuel,f
0
L/4
L+0.05L
L

Figure4

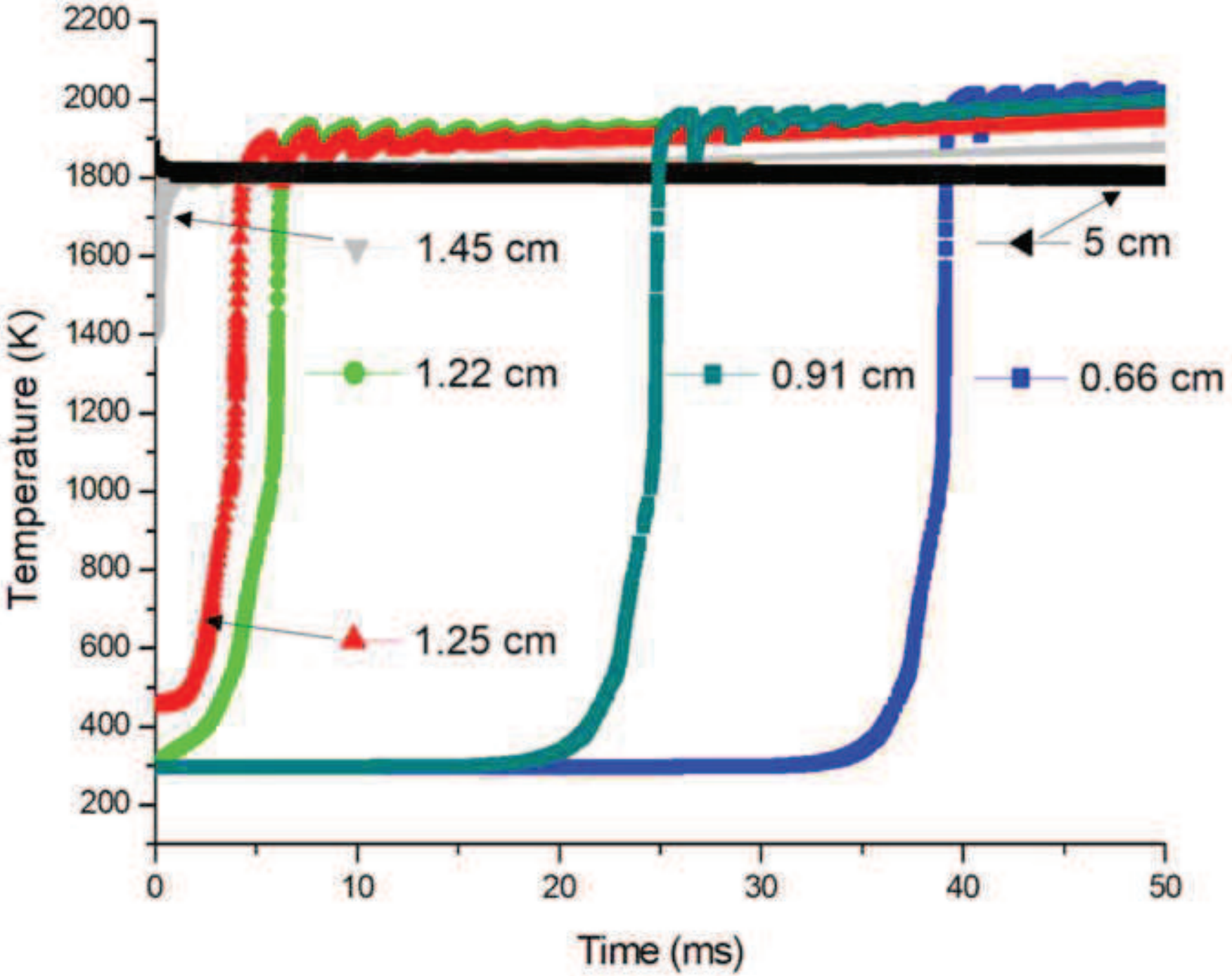
Temperature (K)
2200
2000
1800
1600
1400
1200
1000
800
600
400
200
0
10
20
30
40
50
Time (ms)
1.45 cm
1.22 cm
1.25 cm
0.91 cm
5 cm
0.66 cm

Figure5

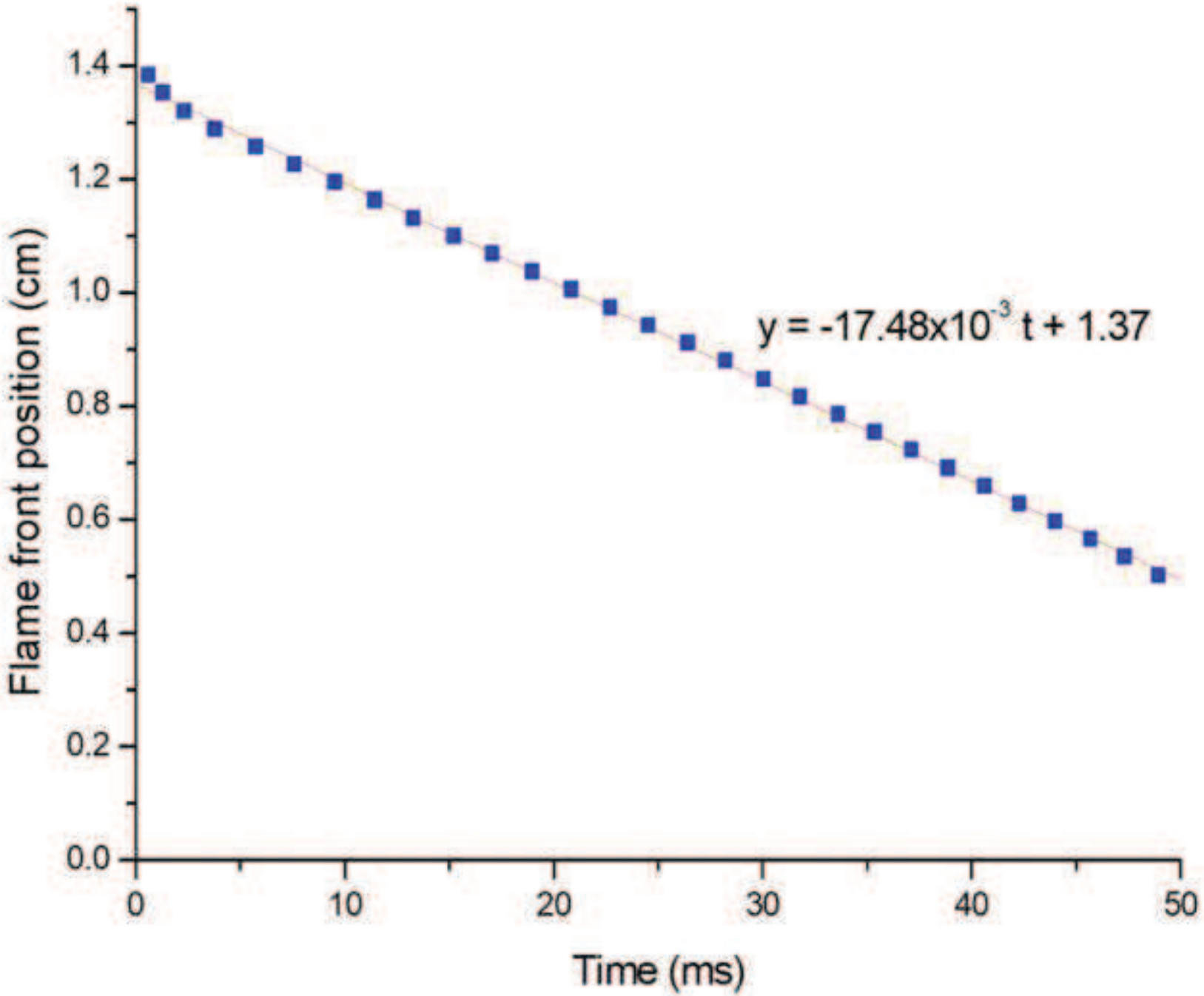
Flame front position (cm)
1.4
1.2
1.0
0.8
0.6
0.4
0.2
0.0
y = -17.48x10-3 t + 1.37
0
10
20
30
40
50
Time (ms)

Figure6

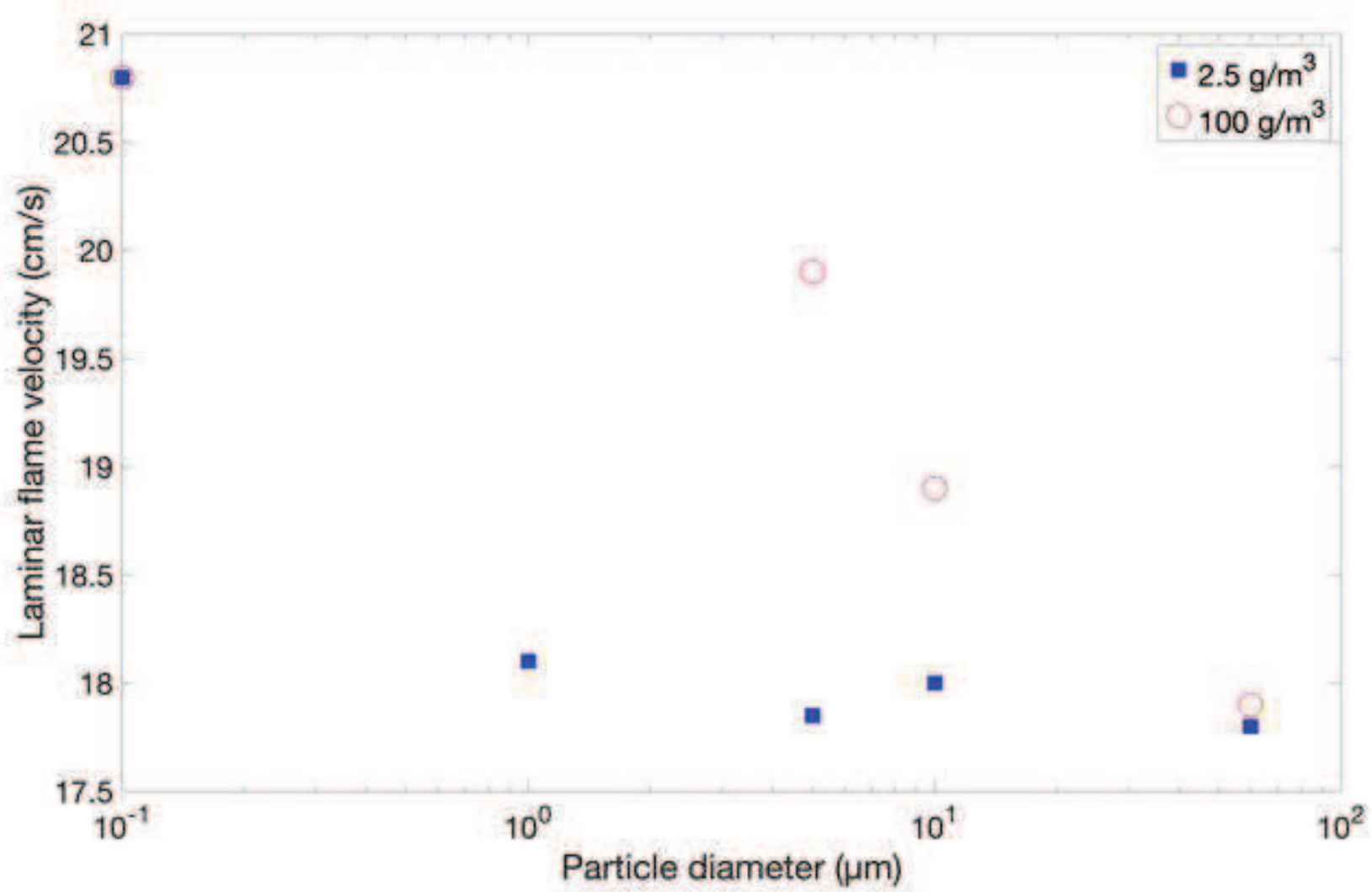
Laminar flame velocity (cm/s)
21
20.5
20
19.5
19
18.5
18
17.5
10^{-1}
10^{0}
10^{1}
10^{2}
Particle diameter (μm)
2.5 g/m^3
100 g/m^3

Figure7

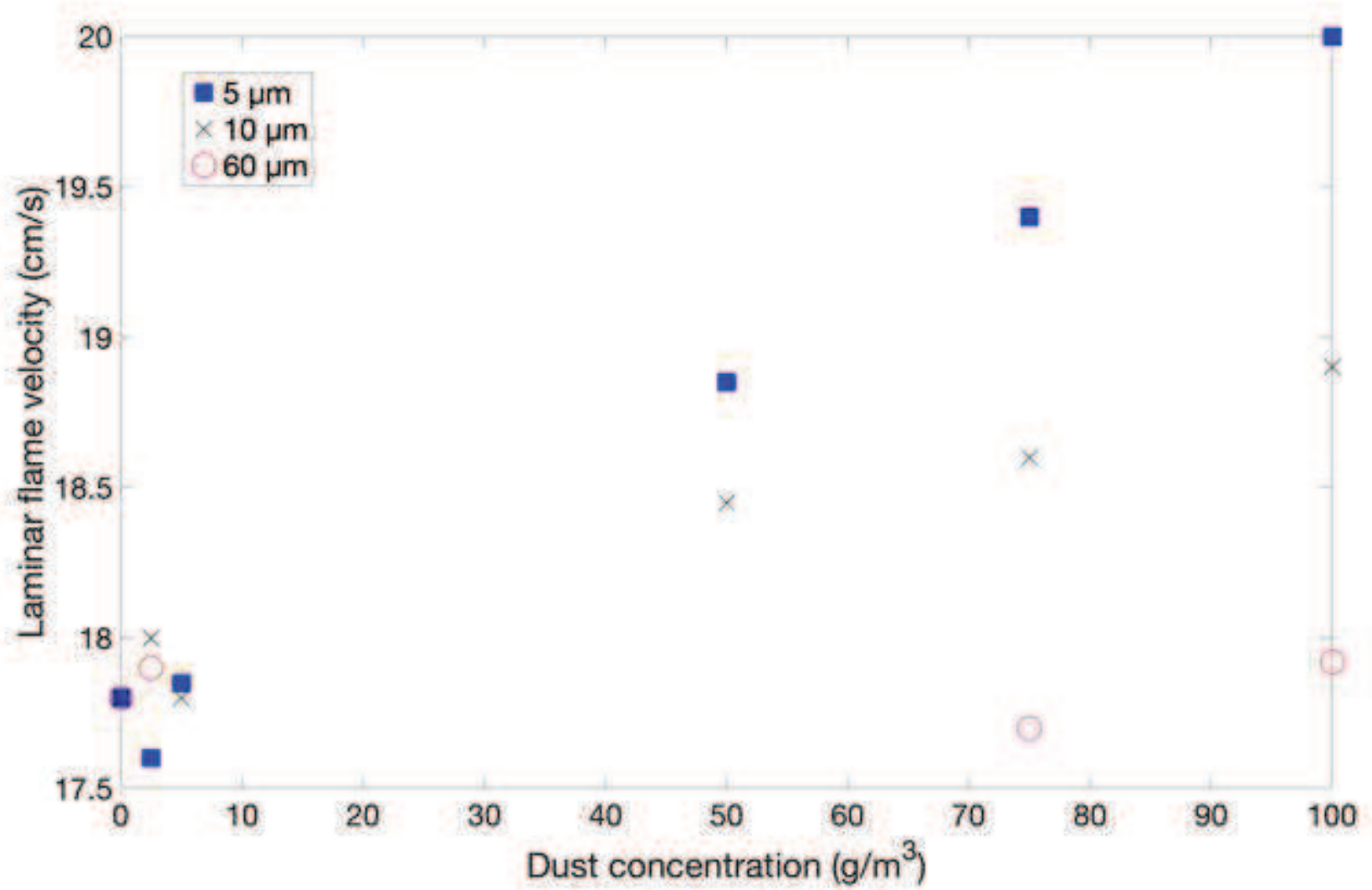
5 μm
10 μm
60 μm
Laminar flame velocity (cm/s)
Dust concentration (g/m3)
20
19.5
19
18.5
18
17.5
0
10
20
30
40
50
60
70
80
90
100

Figure8

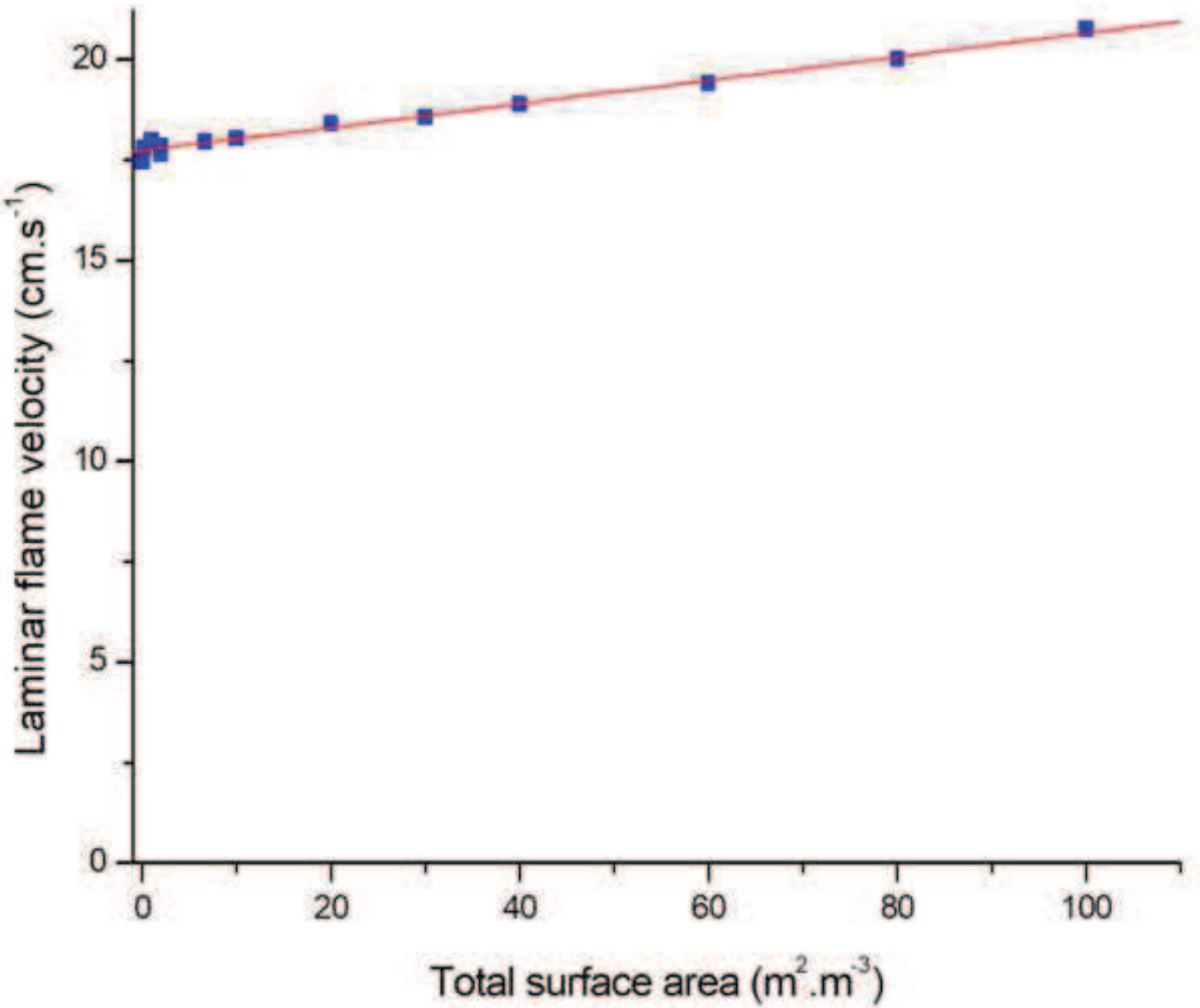
Laminar flame velocity (cm.s-1)
0
5
10
15
20
0
20
40
60
80
100
Total surface area (m2.m-3)